Interpreting the Mg II h and k Line Profiles of Mira Variables

B. E. Wood[1], M. Karovska

Harvard-Smithsonian Center for Astrophysics, 60 Garden St., Cambridge, MA 02138.

wood@head-cfa.harvard.edu, karovska@head-cfa.harvard.edu

ABSTRACT

We use radiative transfer calculations to reproduce the basic appearance of Mg II lines observed from Mira variables. These lines have centroids that are blueshifted by at least 30 km s^{-1} from the stellar rest frame. It is unlikely that flow velocities in the stellar atmospheres are this fast, so radiative transfer effects must be responsible for this behavior. Published hydrodynamic models predict the existence of cool, downflowing material above the shocked material responsible for the Mg II emission, and we demonstrate that scattering in this layer can result in Mg II profiles as highly blueshifted as those that are observed. However, our models also show that scattering *within* the shock plays an equally strong role in shaping the Mg II profiles, and our calculations illustrate the importance of partial redistribution and the effects of being out of ionization equilibrium.

Subject headings: stars: AGB and post-AGB — stars: variables: other — stars: oscillations — ultraviolet: stars — line: profiles

1. Introduction

Mira variables are an important class of pulsating variable stars representing the final stages in the life of a solar-type star. The stellar pulsation of these stars drives periodic shock waves through their atmospheres. These shocks waves determine the atmospheric structure of Miras to a large extent, and they assist in producing very high mass loss rates. The Mg II h & k lines of Mira variables at 2802.705 Å and 2795.528 Å, respectively, are useful diagnostics for the shocks, since they are produced within the heated plasma just behind the outwardly-propagating shocks.

Wood & Karovska (2000, hereafter Paper 1) analyzed IUE observations of several extensively observed Mira variables in order to study the properties of their UV emission lines, especially Mg II h & k. Figure 1 shows a sequence of IUE spectra of the Mira variable R Car, illustrating how the Mg II h line profile typically varies during the course of a pulsation cycle. The Mg II flux rises well

[1]Present address: JILA, University of Colorado, Boulder, CO 80309-0440.

after optical maximum ($\phi = 0.0$), peaking near $\phi = 0.2 - 0.5$ and then decreasing (see also Brugel, Willson, & Bowen 1990; Luttermoser 1996). Although this pattern is observed for every pulsation cycle, the amount of Mg II flux produced during a pulsation cycle can vary greatly from one cycle to the next.

The Mg II k lines are almost always contaminated with absorption lines of Fe I and Mn I, indicating the existence of overlying cool material above the Mg II emission region. The Mg II h line, however, is not greatly contaminated by such absorption. Thus, most of this paper (and Paper 1) focuses on the more pristine h line profile.

The centroid of the Mg II h line is always highly blueshifted by at least 30 km s^{-1} from the rest frame of the star, and the magnitude of the blueshift is clearly observed to decrease with pulsation phase, as seen in Figure 1. The blueshifts vary somewhat from star to star and cycle to cycle, but typical centroid changes are from -70 km s^{-1} to -40 km s^{-1} from $\phi = 0.2$ to $\phi = 0.6$ (see Paper 1). This behavior is very similar to that of the optical Ca II H & K lines (Merrill 1960). The width of the Mg II h line is also phase-dependent, decreasing from about 70 km s^{-1} to about 40 km s^{-1} between $\phi = 0.2$ and $\phi = 0.6$ (see Fig. 1).

In addition to Mg II h & k, many multiplets of Fe II lines are observed in the UV spectra of Miras. Another useful line detected in these data is the Al II] λ2669 line. The fluxes of the Fe II and Al II] lines exhibit the same phase-dependent behavior as the Mg II lines, but their widths and centroid velocities are of a different character. The Fe II and Al II] lines have very narrow widths which are not phase-dependent. Except for Fe II λ2599 (see below), the Fe II and Al II] lines of most of the Miras show modest blueshifts of $5 - 15$ km s^{-1}, which are not variable within the error bars. In this paper, we use simple radiative transfer calculations of Mg II line profiles to try to explain why the Mg II lines are broader and have much larger blueshifts than the less optically thick Fe II and Al II] lines.

2. Possible Explanations for the Mg II Line Shifts

The Fe II and Al II] lines will have significantly lower opacities than the much stronger Mg II h & k lines, and some may even be optically thin (Carpenter, Robinson, & Judge 1995). This opacity difference is presumably the primary reason for the behavioral differences of these lines. Evidence for this is provided by the most optically thick Fe II line at 2599.394 Å, which behaves differently from the other Fe II lines and in fact exhibits some of the characteristics of Mg II h & k, with larger line widths and large blueshifts (Paper 1).

Because of their low opacity, the Fe II and Al II] line centroids should be more indicative of the true outflow velocities of the shocked material, and the line widths should be more indicative of turbulent velocities within the shocked material. In the following, we explore possible reasons why the Mg II lines are broader and more blueshifted.

Models and observations of various stellar sources demonstrate that as the opacity in an emission line is increased, the line typically broadens and separates into two peaks (e.g. Robinson, Carpenter, & Brown 1998). This is why solar Lyman-α, Mg II h & k, and Ca II H & K lines are observed to be double-peaked (Feldman & Doschek 1977). Many Mg II lines of red giant and supergiant stars are also double-peaked, although the blue peak is often affected by wind absorption (Robinson & Carpenter 1995). For Miras, perhaps we are seeing only the blue peak of the Mg II emission, with the red peak being suppressed by overlying material.

One possible reason why only the blue peak is visible is that circumstellar neutral material is completely absorbing the red peak. The observed Mg II k lines of Miras are clearly affected by this overlying neutral material (see Paper 1). However, this interpretation requires far more neutral absorption on the red side of the line than on the blue side for both the h and k lines. This would also have to be the case for the Ca II H & K lines, which behave similarly to Mg II h & k; and also for the Fe II λ2599 line to explain its larger blueshift. It seems very unlikely that neutral absorption features would blanket predominantly the red sides of *all* these lines. The suppression of the red peak must therefore be due to radiative transfer processes within the lines themselves.

The simplest explanation is that there is downflowing Mg II material suppressing the emission produced by outflowing Mg II material. Hydrodynamic models of pulsating Miras suggest that after material is accelerated outwards by shocks it will gravitationally decelerate and fall back towards the star, meaning there should be downflowing material present above the pulsation-induced shocks (Bowen 1988; Bessell, Scholz, & Wood 1996; Höfner et al. 1998).

Kraft (1957) used such a scenario to try to explain the behavior of Ca II H & K lines observed from Cepheids and Miras. He assumed that an overlying absorption layer of downflowing Ca II material obliterates the red side of the Ca II lines. One problem with this simple model is that unless densities in the downflowing material are many orders of magnitude higher than one would expect based on the hydrodynamic models, the layer should be a scattering layer and not an absorption layer. At the relatively low densities that are expected to exist in this region of the atmosphere, there is no immediately apparent way to destroy/absorb Mg II photons. In principle, a highly opaque scattering layer might also work, but in a scattering environment it is harder to completely suppress the entire red side of a line since photons can frequency scatter far enough into the red wing of the line to escape the layer. In order to test whether a reasonable downflowing scattering layer can in fact suppress the red peaks of the Mg II lines, we perform the following radiative transfer simulation.

3. Radiative Transfer Calculations

3.1. Methodology

The hydrodynamic models of pulsating Miras show that the pulsation produces a series of outwardly-propagating shocks within the outer atmosphere of these stars. In Figure 2a-c, we show schematic density, temperature, and velocity profiles that represent the innermost shock of a pulsating Mira and the region overlying it, which extends nearly to the next shock. These curves are meant to be crudely similar to the model results of Bowen (1988) and Willson & Bowen (1988) at a pulsation phase of about $\phi = 0.5$. In practice, we experimented with minor adjustments to all these curves in order to find a model that adequately reproduced the observations. The density, temperature, and velocity structure of the atmosphere all play a role in determining the properties of the Mg II profiles.

We computed the ionization state of the model atmosphere in Figure 2 using collisional ionization rates from Voronov (1997) and recombination rates from Shull & Van Steenberg (1982). In computing the electron density we consider all abundant elements whose ionization might contribute significant numbers of electrons. We assume the solar abundances of Anders & Grevesse (1989) for these calculations. Magnesium, hydrogen, silicon, and iron turn out to be the dominant electron contributors.

The thin lines in Figure 2d show the electron density and Mg II density computed assuming ionization equilibrium. However, ionization equilibrium is not a good approximation for this dynamic atmosphere. Typical atomic recombination rates are $\alpha \sim 10^{-12}$ cm^3 s^{-1} for the temperatures within the model atmosphere. The recombination timescale is $t_r = (n_e \alpha)^{-1}$. For electron densities below $n_e = 3 \times 10^4$ cm^{-3}, t_r is longer than most Mira pulsation periods. Recombination will not have time to occur when the electron density approaches this value, so the plasma outside the shocks will be frozen in a much higher ionization state than suggested by the ionization equilibrium calculations (see Fig. 2d).

In order to estimate more reasonable electron and Mg II densities, we performed the following simulation. Ignoring the velocity structure implied by Figure 2c, we followed the ionization state of a static parcel of gas as we repeatedly ran the density and temperature profiles of Figures 2a-b over the parcel with a period of 300 days, a typical Mira pulsation period. The electron density of the parcel was initially set to some arbitrary value. At the temperatures with which we are concerned, we can assume each atom is either neutral or singly-ionized. Collisional ionization and radiative recombination are the two processes responsible for establishing the ionization state of each element, and the equation

$$\frac{dn_2}{dt} = n_e \left(n_1 C_{12} - n_2 \alpha_{21} \right) \tag{1}$$

shows how the density of the ionized state of the element in question (n_2) changes due to these processes, where n_1 is the density of the neutral state of the element, and C_{12} and α_{21} are the temperature dependent ionization and recombination rates to and from the singly ionized state,

respectively. By solving this simple differential equation, we can express the time dependent density of the singly-ionized state of a given element after a time step Δt as

$$n_2(t+\Delta t) = \frac{n_{tot}C_{12}}{C_{12}+\alpha_{21}} + \left(n_2(t) - \frac{n_{tot}C_{12}}{C_{12}+\alpha_{21}}\right) \exp\left(-n_e(t)\,(C_{12}+\alpha_{21})\,\Delta t\right), \tag{2}$$

where n_{tot} is the total number density of the element ($n_{tot} = n_1 + n_2$).

The ionization states of each element, and the electron density, are recomputed after each time step. After just a few pulsation cycles, the electron density and ionization states settle into a repeatable pattern, from which we can extract the electron and Mg II density profiles shown as thick lines in Figure 2d. As expected, these densities are very different from the equilibrium values.

We now have all the information we need to compute theoretical Mg II h & k line profiles. Since the observed k line is usually contaminated with neutral absorption features (see Paper 1), we focus on the h line. We use a simple two-level atom approximation for our calculations. At each level of the atmosphere the number of h line photons generated by collisional excitation per unit volume per unit time is then given (in cgs units) by (e.g., Brown et al. 1984)

$$L = \frac{8.6\times10^{-6}\Omega n_e n}{gT^{0.5}} \exp\left(-\frac{1.44\times10^{8}}{\lambda T}\right), \tag{3}$$

where n is the Mg II number density, Ω is the collision strength, g is the statistical weight of the lower level, and λ is the wavelength of the transition in Ångstroms. For the h line, $\Omega = 5.6$ and $g = 2$ (Mendoza 1981).

The wavelength dependent optical depth for each level of the atmosphere is (e.g., Spitzer 1978)

$$\tau_\lambda(h) = 0.02654 f \int_h^{h_{top}} n(h)\phi_\lambda(h)dh, \tag{4}$$

where f is the oscillator absorption strength, $n(h)$ is the height dependent Mg II density, h_{top} is the height at the top of the atmosphere, and ϕ_λ is the line profile function. For the Mg II h line, $f = 0.3054$ (Morton 1991). The assumed line profile is a Voigt profile with a centroid defined by the velocity profile in Figure 2c, and a width defined by a height-dependent microturbulence function, $b(h)$, also shown in Figure 2c. As the figure shows, we assume a microturbulence of 5 km s^{-1} inside the shock and 3 km s^{-1} outside, although in practice we experiment with different values (see below).

Because the critical density where the collisional deexcitation rate equals that of radiative deexcitation ($n_{crit} \approx 5\times10^{14}$ cm^{-3}) is at least 10^9 times higher than the densities in our model atmosphere, we neglect collisional deexcitation in our calculations, making this truly a pure scattering atmosphere. We assume complete angular redistribution for each scattering event, but for the frequency redistribution we experiment with both complete redistribution (CRD) and partial redistribution (PRD). In the PRD treatment, the redistribution function defining the probability

of a photon absorbed with frequency ν being reemitted with frequency ν' in a comoving rest frame can be expressed as (e.g. Milkey & Mihalas 1973; Basri 1980)

$$R(\nu,\nu') = (1-\Lambda)R_{II}(\nu,\nu') + \Lambda R_{III}(\nu,\nu'), \tag{5}$$

where R_{II} and R_{III} are the integral functions first defined by Hummer (1962). The Λ paramenter is

$$\Lambda = \frac{\Gamma_{col}}{\Gamma_{col}+\Gamma_{rad}}, \tag{6}$$

where Γ_{col} and Γ_{rad} are the collisional and radiative damping parameters, respectively. However, for our model atmosphere collision rates are very low because densities are very low. As a consequence, Γ_{col} and Λ are both very small; we estimate $\Lambda \sim 10^{-8}$ at most. Thus, for our purposes, $R(\nu,\nu') \approx R_{II}(\nu,\nu')$ is a very good approximation.

Several techniques have been used in the past to evaluate the complex R_{II} integral. Adams, Hummer, & Rybicki (1971) presented a method of simplifying the integral using polynomial series expansions. Kneer (1975) proposed an even simpler technique, which is still widely used (e.g. Vernazza, Avrett, & Loeser 1981; Luttermoser et al. 1989). However, Basri (1980) questions the accuracy of the Kneer approximation for supergiant atmospheres, so in our calculations we evaluate R_{II} by direct numerical integration.

We adopt a simple Monte Carlo approach for the radiative transfer calculations. Individual photons created by collisional excitation are followed from one scattering event to the next until they escape the scattering layer. For each scattering event, we shift to the rest frame of the scattering layer in order to ensure the frequency redistribution is done correctly. For a layer as opaque as the one modeled here, each photon scatters an average of roughly 10,000 times before escaping. By keeping track of where the photons scatter, we gradually build up a wavelength and height dependent source function, S_λ. We also keep track of the trajectory angle θ of escaping photons relative to the normal of our plane-parallel atmosphere. Combining this information and the source function, we compute line profiles for various values of $\mu = \cos\theta$ using the familiar radiative transfer equation

$$I_\lambda(\tau=0,\mu) = \frac{1}{\mu}\int_0^{\tau_\lambda} S_\lambda(t)e^{-t/\mu}dt. \tag{7}$$

We then compute a final disk-integrated line profile using a routine from Valenti & Piskunov (1996). The disk integration procedure is really only valid for thin atmospheres, which will not be the case here. However, we are only interested in the gross appearance of the line profile rather than its exact flux or center-to-limb behavior, so our plane-parallel treatment and the disk integration procedure just described should be good enough for our purposes.

3.2. Results

After experimenting with many modest modifications to the assumed density, temperature, velocity, and microturbulence structure of our model atmosphere, we settled on the curves shown

in Figures 2a-c. An optically thin Mg II line produced by the model atmosphere in Figure 2 has a centroid velocity of about -15 km s^{-1}, which is a bit large but is still within the range of centroid velocities observed for the Fe II and Al II] lines (see §1). The wavelength integrated surface flux derived for our best-fit model profile is 147 ergs cm^{-2} s^{-1}. If we convert this into an observed flux assuming a stellar radius of 2 AU and a stellar distance of 100 pc, which are typical values for the Miras studied in Paper 1 (see also Karovska et al. 1991, 1997; Burns et al. 1998), we find a predicted flux at Earth of 1.4×10^{-12} ergs cm^{-2} s^{-1}. This flux is nicely within the range of observed values at $\phi = 0.5$ (see Paper 1).

Figure 3a shows the model Mg II h line profile after convolution with IUE's instrumental profile, which has a width of 0.2 Å. Two observed Mg II h lines are also shown in Figure 3a for the sake of comparison, one from R Car (dotted line) and one from T Cep (dashed line). Both are observations near $\phi = 0.5$. The originally computed model profile was significantly narrower than the observed profiles, so we had to broaden it by assuming a macroturbulence of 10 km s^{-1} in order to obtain the profile shown in the figure, which is a reasonably good match to the observations. The model profile still has a weak red peak, but this is not grossly inconsistent with observations since the observed R Car profile appears to have a similar feature. The centroid of the model profile is at about -33 km s^{-1}, consistent with the velocities typically observed around $\phi = 0.5$ (see Paper 1).

It was not an easy matter to find a combination of density, temperature, velocity, and microturbulence profiles which would suppress the red peak to the required degree while still maintaining a velocity structure consistent with the velocities of the optically thin Fe II and Al II] lines and also producing roughly the correct amount of Mg II flux. Increasing or decreasing the assumed densities by a factor of 2, for example, is enough to significantly increase the flux in the red peak of the model Mg II line, degrading the agreement with the observations. It is not clear at all why the atmospheric structure of Miras should be so finely tuned, so it is quite possible that our models are still lacking some characteristic that is important for determining the observed line profiles. Nevertheless, the identification of at least one model that adequately fits the data is enough to demonstrate that scattering in an atmospheric structure like that shown in Figure 2, with downflowing material above the shock, can in principle produce the observed Mg II profiles without any need for absorption from overlying material. We have found we can best reproduce the observed profiles if the microturbulence of the downflowing material is assumed to be lower than that of the shocked material responsible for the emission, although models with $b = 6$ km s^{-1} or $b = 1$ km s^{-1} outside the shock are not dramatically worse than the best models with $b = 3$ km s^{-1} outside the shock.

In Figure 3b, our best-fit profile is compared with two other model profiles: a profile computed using CRD rather than PRD (dotted line), and a profile computed using the ionization equilibrium densities in Figure 2d (dashed line) instead of our preferred estimates of non-equilibrium densities. A more substantial red peak is prominent in each of these profiles, so they do not agree with the observations as well as our best model.

The computations assuming ionization equilibrium do not do as well simply because there is no Mg II in the downflowing material above the shock that can scatter red peak photons (see Fig. 2d). All the magnesium is in its neutral state due to the low temperatures present there. It is interesting to note, however, that a strong blue peak asymmetry results even in the absence of scattering from downflowing material. Much of the suppression of the red peak is therefore due to scattering within the shock itself. Most of the emergent photons naturally scatter last in the near side of the shock, suggesting that the positive velocity gradient at that location helps suppress the red peak all by itself, although adding scattering from the downflowing material (i.e., switching to the non-equilibrium model in Fig. 3) does suppress the red peak even further.

The CRD calculations fail to reproduce the observations because it is too easy for photons to scatter into the far wings of the line, past the spectral region where the downflowing material can scatter the photons and prevent their escape. Thus, CRD computations do not dramatically suppress the red peak of the line and the resulting profile is extremely broad. Previous work has demonstrated that CRD is a very poor approximation for red giant and supergiant atmospheres and generally produces unrealistically broad Mg II lines (Basri 1980; Drake & Linsky 1983; Luttermoser et al. 1989).

Although we have succeeded in roughly reproducing the Mg II line profiles, there is one possible problem with the model, and that is that it produces an h line profile that is too narrow. As mentioned above, we corrected this by adding macroturbulent line broadening, but the presence of such macroturbulence may also broaden less opaque lines to a similar extent, depending on whether the macroturbulence exists where the Mg II lines are originally formed or in higher layers of the atmosphere where the emission is scattered. In any case, this model may not be able to reproduce the narrow profiles of the Fe II and Al II] lines, which are much less opaque than Mg II h & k if not actually optically thin. It is possible that the narrow model profile reflects inaccuracies introduced into the calculation by the various assumptions that have been made (i.e., the plane-parallel approximation and crude disk integration technique) rather than the existence of macroturbulent flow fields.

Despite the potential difficulty just described, we conclude that it is possible in principle for atmospheric structures like those predicted by hydrodynamic models of Miras to account for the lack of red peaks in observed Mg II profiles from these pulsating stars. Further modeling is needed to confirm these results, and to find a model which accurately reproduces the profiles of both Mg II h & k and of the less optically thick Fe II and Al II] lines. In addition, future modeling could combine hydrodynamic modeling and a more sophisticated treatment of the radiative transfer in a self-consistent manner.

4. Summary

The large blueshifts of the centroids of Mira Mg II lines are unlikely to be indicative of mass motions this rapid, because less optically thick lines suggest more modest flow velocities. The Mg II k line is clearly contaminated by absorption from overlying material, but this contamination does not explain the large blueshifts, since the blueshifts are seen not only for the Mg II h & k lines but also for the Ca II H & K lines, and the probability of overlying absorption producing similar blueshifts in all four very opaque lines is very small. We have used radiative transfer calculations to determine if shock structures such as those suggested by published hydrodynamic models of Miras (e.g. Bowen 1988) can generate Mg II h line profiles like those observed by IUE. In particular, we test whether downflowing material above the shocks, such as that predicted by the models, can suppress the red side of the emission lines, thereby producing highly blueshifted profiles like those that are observed. We find that scattering in such an atmosphere can reproduce the observed Mg II profiles and fluxes under the following conditions:

1. Calculations assuming complete redistribution cannot reproduce the observed profiles. The effects of partial redistribution must be taken into account.

2. Simple estimates of recombination timescales suggest the plasma outside the shocks is out of ionization equilibrium, and our attempt to correct for these effects improves the agreement between the observed and modeled Mg II profiles. However, a strong blue peak asymmetry results even when equilibrium densities are assumed and there is no scattering from the overlying downflowing material. This suggests that scattering *within* the shock accounts for much of the suppression of the red side of the line.

3. Although the velocity predicted for optically thin lines in our model is consistent with observed velocities of Fe II and Al II] lines, there may be a problem with the line widths. We had to assume a macroturbulence of 10 km s^{-1} to broaden our model Mg II profile enough to be consistent with observations, but the existence of such macroturbulence would possibly broaden the Fe II and Al II] lines more than is observed. More sophisticated modeling in the future could resolve this issue.

Understanding the gross properties of the observed Mg II lines is a necessary first step before trying to understand the phase-dependent behavior described in Paper 1. Phase-dependent changes in density, temperature, velocity, microturbulence, and macroturbulence may all play a role in producing this behavior.

We wish to thank the referee, R. Robinson, for comments which improved the paper. MK is a member of the Chandra Science Center, which is operated under contract NAS-839073, and is partially supported by NASA.

REFERENCES

Adams, T. F., Hummer, D. G., & Rybicki, G. B. 1971, J. Quant. Spec. Radiat. Transf., 11, 1365

Anders, E, & Grevesse, N. 1989, Geochim. Cosmochim. Acta, 53, 197

Basri, G. S. 1980, ApJ, 242, 1133

Bessell, M. S., Scholz, M., & Wood, P. R. 1996, A&A, 307, 481

Bowen, G. H. 1988, ApJ, 329, 299

Brown, A., Jordan, C., Stencel, R. E., Linsky, J. L., & Ayres, T. R. 1984, ApJ, 283, 731

Brugel, E. W., Willson, L. A., & Bowen, G. 1990, in Evolution in Astrophysics: IUE Astronomy in the Era of New Space Missions, (Noordwijk: ESA SP-310), 241

Burns, D., et al. 1998, MNRAS, 297, 462

Carpenter, K. G., Robinson, R. D., & Judge, P. G. 1995, ApJ, 444, 424

Drake, S. A., & Linsky, J. L. 1983, ApJ, 273, 299

Feldman, U., & Doschek, G. A. 1977, ApJ, 212, L147

Gillet, D. 1988, A&A, 190, 200

Hinkle, K. H., Lebzelter, T., & Scharlach, W. W. G. 1997, AJ, 114, 2686

Höfner, S., Jørgensen, U. G., Loidl, R., & Aringer, B. 1998, A&A, 340, 497

Hummer, D. G. 1962, MNRAS, 125, 21

Karovska, M., Hack, W., Raymond, J., & Guinan, E. 1997, 482, L175

Karovska, M., Nisenson, P., Papaliolios, C., & Boyle, R. P. 1991, ApJ, 374, L51

Kneer, F. 1975, ApJ, 200, 367

Kraft, R. P. 1957, ApJ, 125, 336

Luttermoser, D. G. 1996, in Cool Stars, Stellar Systems, and the Sun, Ninth Workshop, ed. R. Pallavicini & A. K. Dupree (San Fransisco: ASP Conf. Ser., Vol. 109), 535

Luttermoser, D. G., Johnson, H. R., Avrett, E. H., & Loeser, R. 1989, ApJ, 345, 543

Mendoza, C. 1981, J. Phys. B, 14, 246

Merrill, P. W. 1960, in Stellar Atmospheres, ed. J. L. Greenstein (Chicago: The Univ. of Chicago Press), 509

Milkey, R. W., & Mihalas, D. 1973, ApJ, 185, 709

Morton, D. C. 1991, ApJS, 77, 119

Robinson, R. D., & Carpenter, K. G. 1995, ApJ, 442, 328

Robinson, R. D., Carpenter, K. G., & Brown, A. 1998, ApJ, 503, 396

Shull, J. M., & Van Steenberg, M. 1982, ApJS, 48, 95

Spitzer, L. 1978, Physical Processes in the Interstellar Medium (New York: John Wiley & Sons)

Valenti, J. A., & Piskunov, N. 1996, A&AS, 118, 595

Vernazza, J. E., Avrett, E. H., & Loeser, R. 1981, ApJS, 45, 635

Voronov, G. S. 1997, Atomic Data and Nuclear Data Tables, 65, 1

Willson, L. A., & Bowen, G. H. 1988, in Polarized Radiation of Circumstellar Origin, (Tucson: Univ. of Arizona Press), 485

Wood, B. E., & Karovska, M. 2000, ApJ, to appear May 20 (Paper 1)

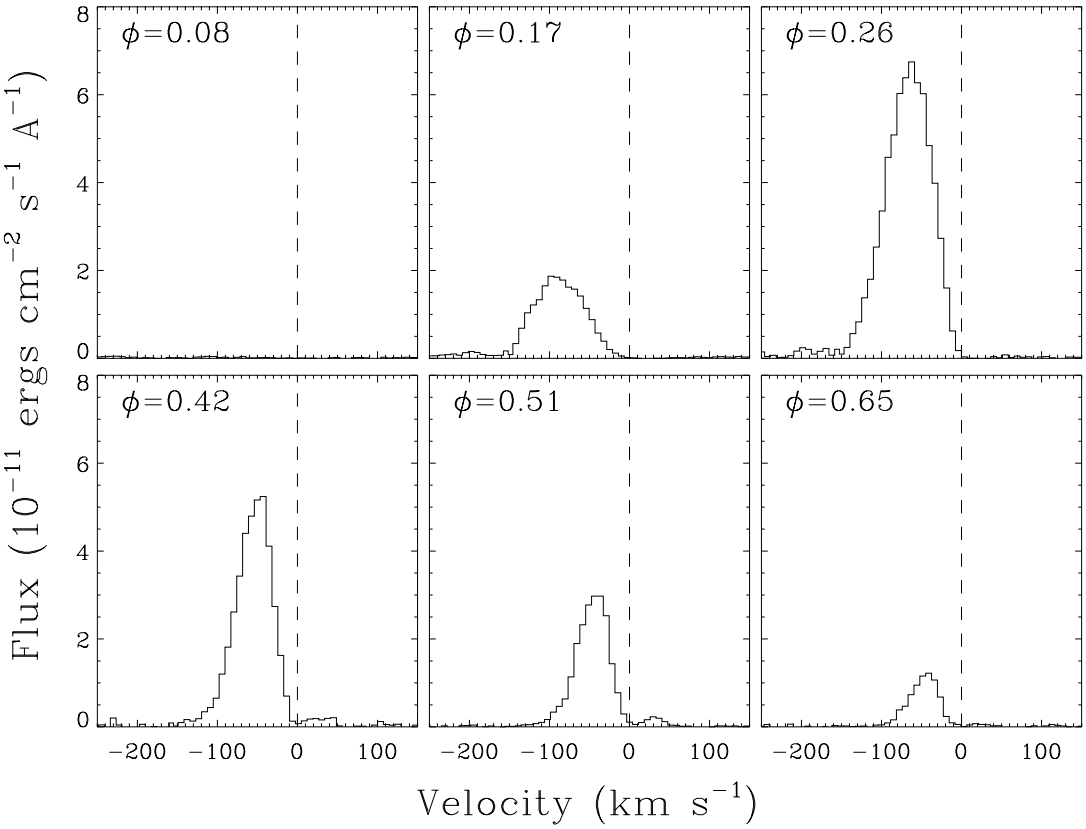

Fig. 1.— A sequence of IUE spectra of the Mg II h line observed in 1989-1990 from the Mira variable R Car, illustrating how the profile typically varies during the course of a pulsation cycle. The spectra are plotted on a velocity scale in the stellar rest frame.

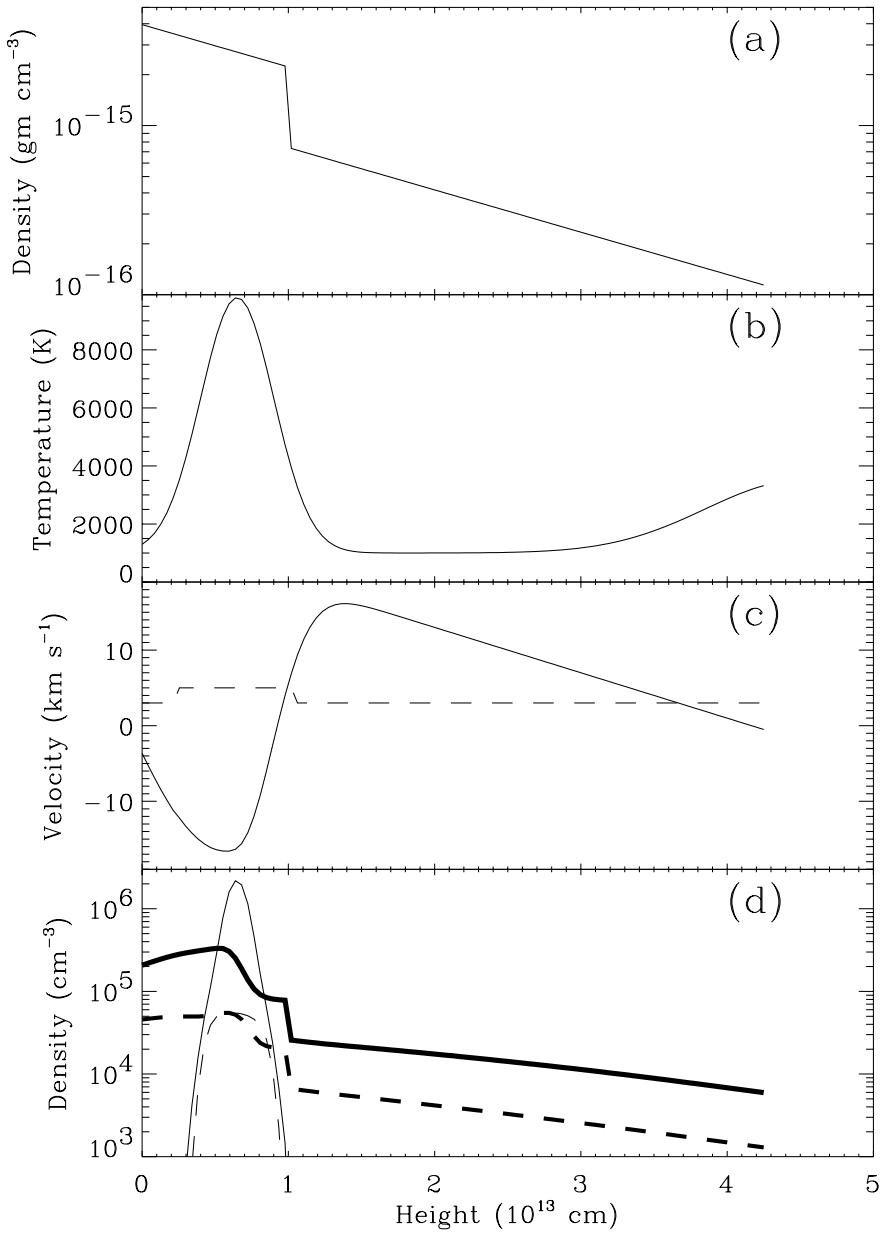

Fig. 2.— A schematic model of the innermost shock of a pulsating Mira and the region overlying it. The density, temperature, and flow velocity are shown as solid lines in panels (a)-(c). Panel (c) also displays the assumed microturbulent velocity profile for our "best-fit" radiative transfer model (dashed line). Panel (d) displays two estimates of the electron density (solid lines) and the Mg II density (dashed lines), one which assumes ionization equilibrium (thin lines), and one which attempts to correct for non-equilibrium effects (thick lines).

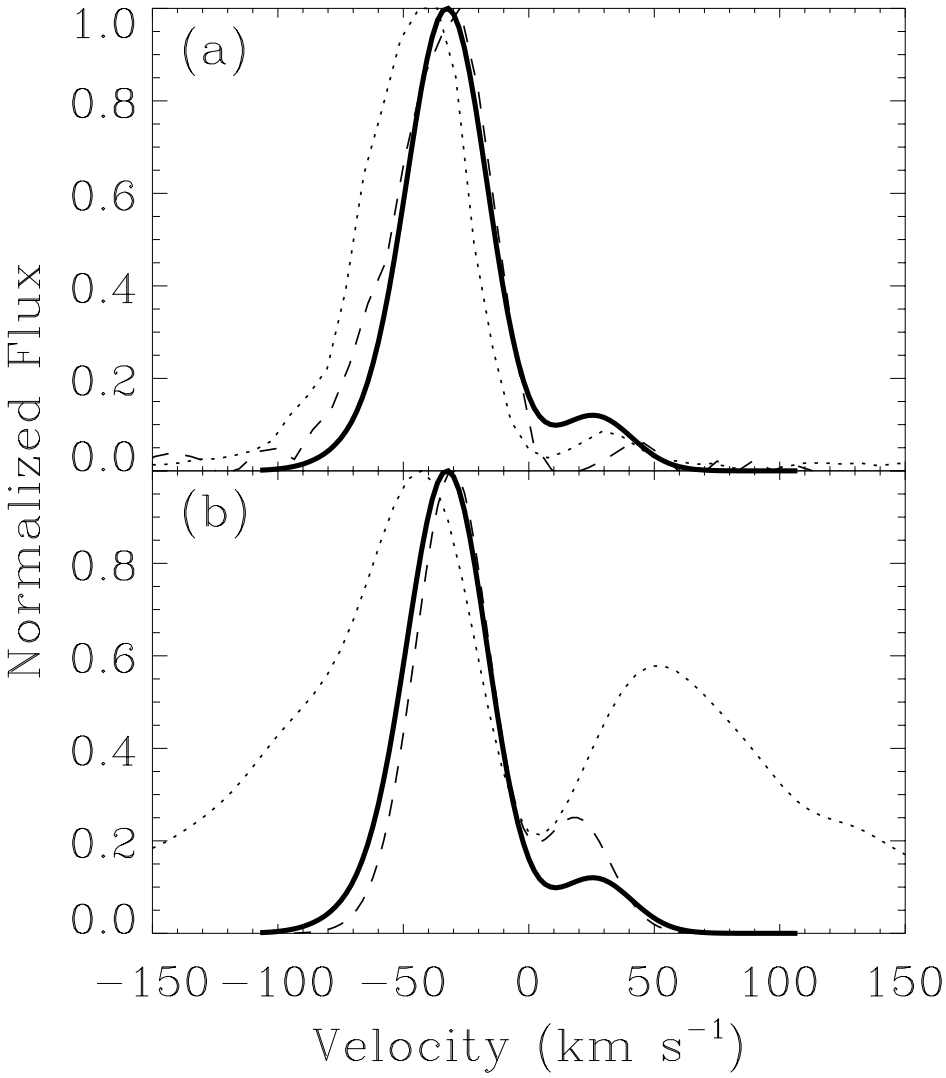

Fig. 3.— (a) Our "best-fit" model Mg II h line profile (solid line) compared with two observed profiles, one from R Car (dotted line) and one from T Cep (dashed line). (b) In this panel, the same best-fit profile from (a) is compared with two other model profiles: a profile computed using CRD rather than PRD (dotted line), and a profile computed assuming ionization equilibrium densities rather than our preferred non-equilibrium densities (dashed line).